



OPTIGRID

D3.1 - Development of DLR analysis and power system models

July 2021

Project Name:	Document Number:	Revision:	Date:
OPTIGRID	D3.1	v1	2020-07-03
Funding:	Authors:	Reviewed by:	Approved by:
Project PTDC/EEI-EEE/31711/2017 funded by national funds through the budget of the Foundation for Science and Technology (FCT) *	Hugo Algarvio Joaquim Duque António Couto	Joaquim Duque	Ana Estanqueiro

Revisions in this document:

First version

*Project PTDC/EEI-EEE/31711/2017 submitted under the call for tenders (AAC) No. 02 / SAICT / 2017, and funded by national funds through the budget of the Foundation for Science and Technology (FCT).

Executive Summary

This deliverable presents the work developed by LNEG as part of the R&D activities of the project *OPTIGRID - Methodology for the dynamic line rating analysis and optimal management of power networks*. According to the plan activities of Tasks 3.1 and 3.2, the main objective of this deliverable is to integrate the mathematical model for the Dynamic Line Rating (DLR) analysis in the optimal power flow model for a generic AC power system, previously developed in LNEG.

The main limiting factor for the transmission capacity of overhead lines (OHLs) is usually defined by a thermal constraint. For OHLs several effects are present, some with a positive contribution while others can lead to the potential congestion of the electrical networks. The seasonal line rating (SLR) methodology, traditionally used by the system operators to ensure that the grid does not operate over the maximum pre-defined conductor temperature, determines the line's ampacity from constant weather conditions using: 1) seasonal basis information or 2) conservative weather conditions. These conditions usually underestimate the real transmission capacity of OHLs. Thus DLR analysis allows assessing more realistic current limits for the power lines could present a method to deal with potentially congested electrical networks enabling the optimal integration of distributed renewable power generation.

Table of Contents

1.	Introduction	4
2.	Dynamic Line Rating Methodology	6
2.1	Heating Effects.....	8
2.1.1	Joule heating	8
2.1.2	Magnetic Heating	8
2.1.3	Solar heating	9
2.1.4	Corona heating.....	10
2.2	Cooling Effects.....	10
2.2.1	Convective cooling.....	10
2.2.2	Forced convectional cooling.....	12
2.2.3	Natural convective cooling.....	13
2.2.4	Convective cooling at reduced wind speeds.....	14
2.2.5	Radiative cooling.....	14
2.2.6	Evaporative cooling.....	14
2.3	Wind incident angle on overhead lines	15
3.	Optimal power flow	16
4.	Assessment of dynamic electric line capacity using optimal power flow	20
4.1	The Benefits of a coupled DLR and OPF model	20
4.2	The coupled model framework	21
5.	Final remarks	24
6.	References	25

List of Figures

Figure 1: Temporal applications of the coupled DLR and OPF framework.	21
Figure 2: A schematic representation of the coupled model.	22
Figure 3: Temporal application of the coupled DLR and OPF framework.....	24

List of Tables

Table 1: Constants for calculation of forced convection on braided conductors cooled by constant airflow [1].	12
Table 2: Constants for the calculation of the Nusselt number as a function of the angle of incidence of the wind [1].	13
Table 3: Constants for computing natural convection in air conductors [1].	14

1. Introduction

The present deliverable was developed by the Laboratório Nacional de Energia e Geologia (LNEG) as part of the R&D activities of the OptiGRID project - Task 3: Development of models for active high-efficiency electric network operation - that deal with the development and adaptation of the existing mathematical optimization models to perform a network optimized management using a Dynamic Line Rating (DLR) methodology. This report describes the work elaborated in sub-tasks I) *3.1. - Development of mathematical models* and II) *3.2 Development of DLR models*. From that work, two different models were obtained.

The distributed and, generally, remote nature of the renewable energy sources (RES), allied to the need of bringing that energy to distant consumption centres, as cities and industrial parks, raises new challenges to the transmission power systems operators (TSOs). The injection of high levels of RES distributed generation, as is the case for Portugal, can, in some periods, overload the overhead electric power lines (OHLs) of the existing transmission grid. That constitutes a non-admissible occurrence traditionally overcome by upgrading the existing power lines, building new power lines, or limiting RES production, that presents several economic and ecological negative impacts.

To avoid reaching the minimal distance to the ground or to compromise the structural integrity of its cables the overhead power line's temperature is operationally limited. This is done by imposing a limit on the power line capacity computed by a line rating (LR) assessment. The general line rating method performs a cable thermal behaviour analysis by considering all mechanisms contributing to heat up or cooling down the power line cable(s).

Thus, for safety reasons, TSOs use extreme meteorological conditions values to compute the seasonal power line capacity limit, (ampacity)¹, along the guidelines proposed by CIGRÉ Report [1], by IEEE Standard 738 - 2012 [2], or by other proprietary methods. The resulting capacity of those methods is usually referred to as Seasonal Line Rating (SLR). However, the exponential growth of the available computational power enables

¹ The term ampacity (ampere capacity) gives the line's current limit which, given the constant line's tension, is proportional to the capacity limit of the line.

the use of real-time meteorological data to assess the power line ampacity by a DLR method [1], [2]. This method may, according to previous studies and the literature, increment up to 20% of the lines' ampacity values. In the DLR methods, only the most important mechanisms are usually used, namely, the solar and Joule heating effects and the convective cooling effect [3]-[5]. In thermal equilibrium, the effects' actions cancel each other, and the general method gives the methodology for an SLR or a DLR analysis, while if not in a steady-state, the diverse effects actions do not cancel and a temperature change occurs in the power line cable(s). The subsequent thermal evolution may be computed by a quasi-stationary approach if a sufficiently small time-step is used in an iterative process. The main cooling effect, from convection, depends mainly on wind speed. For moderate to high wind speeds the forced convection is dominant and constitutes the main cooling effect. Besides the importance of the wind speed, the angle between the wind and the cable directions (the incidence angle) is also important [2],[5]-[8].

A DLR steady-state numerical model, based on the methodology presented by CIGRE [9] was implemented at LNEG [6]-[8]. According to the working plan of the OptiGRID project, the previous implementation was revised based on the last CIGRE methodology [1] to be applied in the case studies identified in Task 4 of the project [10]. From the simple idea of minimizing the impact associated with the injection of high levels of energy from variable renewable energy sources, mainly wind, on the existing power systems, a strategic decision of using DLR analysis is explored in this deliverable. Given that the high levels of wind power production occur for high levels of its resource, wind, that by convection also cools down the cables of the overhead power lines thus safely allowing for the transport/distribution of higher power levels than the ones determined by the traditional TSO or DSO's (distribution system operator) SLR analyses. The use of DLR analysis may postpone the upgrade of congested power lines or avoid the building of new power lines and thus significantly help reinforce the RES contribution to the existing power systems energy production. During real-time operation, TSOs should be able to rapidly compute the DLR of the overhead lines to safely allow the transit of an ampacity that may go above their lines design's capacity, by just considering the real-time meteorological conditions. The use of the whole methodology for all sectors and lines in a region leads to high computation loads since the DLR of one line can affect the

power flow of an entire region. So, a pre-solver methodology, to be presented in D5.1, was developed to rapidly identify the critical sector of each line required to operate at above 10% of their design's power limit. After this identification, the DLR assessment of each near-overloading line can use only the previously identified critical sector.

To evaluate the DLR methodology proposed, a mathematical model to optimize the power flow (OPF) [11] for the electric grid of a general power system was adapted considering the lines' characteristics, obtained from the DLR, and the technical limitations data made available to the project. The methodology will be applied in Task 5 and the results for the three case studies will be dully reported in D5.1 and D5.2. Section 2 presents the DLR methodology and a complementary methodology to compute the wind incident angle. Section 3 presents the optimal power flow (OPF) formulation. Section 4 presents the framework to assess the DLR analysis of OHLs considering an OPF. Lastly, Section 4 presented the final remarks.

2. Dynamic Line Rating Methodology

The meteorological parameters that may influence the thermal state of an electric overhead conductor include the average speed, the direction, and turbulence of the wind, the ambient temperature, and the solar irradiation. If these parameters and the electric current across the conductor remain stable, then there will be no significant change in the conductor temperature. Under these conditions, the conductor is in thermodynamic equilibrium, *i.e.*, the heat absorbed by the conductor, its thermal gains, equals the heat dissipated by the conductor, its thermal losses, and the conductor is in a steady-state [1],[2],[12] and it obeys the equation:

$$P_J + P_M + P_S + P_i = P_c + P_r + P_w \quad (1)$$

where:

P_J - Joule heating (W / m);

P_M - magnetic heating (W / m);

P_S - solar heating (W / m);

P_i - corona heating (W / m);

P_c - convective cooling (W / m);

P_r - radiative cooling (W / m);

P_w - evaporative cooling (W / m);

Since the different terms do not have the same order of magnitude, it is a common practice to use only the effects that contribute the most, usually P_J , P_M , P_S , P_c and P_r . Given that most power lines use a multi-layered structure the manufacturers set the conductor's layers of cable winding in opposite directions, to reduce the magnetic effects. Thus, the magnetic effects are only important for cables with a steel core and an odd number of layers, in particular one or three layers of aluminium. Given that the maximal temperature limit imposed on the power lines is usually lesser than 90°C the radiative cooling is also comparatively weak and is also not considered in most cases.

If the conductor is not in a steady-state, then equation (1), according to [12], becomes:

$$m c_p \frac{d\bar{T}}{dt} = P_J + P_M + P_S + P_i - P_c - P_r - P_w \quad (2)$$

where:

m - Cable mass per meter (kg/m)

c_p - Specific heat capacity (J/kgK)

T - Cable temperature (K)

t - Time (s)

and the quantity $m c_p \frac{d\bar{T}}{dt}$ represents the cable's net heat transfer. For aluminium cables with a steel core, according to [1], becomes:

$$m c_p = m_a c_{p_a} + m_s c_{p_s} \quad (3)$$

where the index a refers to the aluminium (a non-ferromagnetic material) and s to the steel (a ferromagnetic material).

2.1 Heating Effects

2.1.1 Joule heating

In conductor materials, the passage of a direct current, I_{DC} , faces a resistance, R_{DC} , that causes the heating, P_J , of the conductor material as asserted by Joule's first law $P_J \propto I_{DC}^2 R_{DC}$. In fact, at a microscopic level, the interaction between the current's moving particles and the ionized atoms of the conductor's structure scatters the particles randomizing their movement and therefore reducing their rate of speed along the current direction, i.e., thermalizing the particle motion and increasing the temperature of the system. The values of a conductor's resistance depend on its temperature T . That relation is then used to correct Joule's heating power loss [8]:

$$P_J = I_{DC}^2 R_{DC} [1 + \alpha(\bar{T} - 293.5)] \quad (4)$$

In the above equation, temperatures are in Kelvin and α is the temperature coefficient of resistance per Kelvin degree, R_{DC} , is the direct current value at 20 °C.

The use of the alternate current in power lines induces Eddy currents, inside the electrical conductors, causing the appearance of skin effects that favour the passage of the current closer to the surface at the cost of reducing it at deeper zones of the conductor ([14]). The alternate current resistance, R_{AC} , is now assumed to be proportional to R_{DC} , by a proportionality constant k_j [1], i.e., $R_{AC} = k_j R_{DC}$. Thus, Joule's thermal losses for non-ferromagnetic cables becomes

$$P_J = k_j I^2 R_{DC} [1 + \alpha(\bar{T} - 293.5)] \quad (5)$$

2.1.2 Magnetic Heating

The effect of electromagnetic induction can be significant in steel core electric cables, since in these materials a longitudinal magnetic flux is produced in the steel core, by the current that transits in the conductors of non-ferromagnetic material that cover it [1]. The experimental work developed by [15] with braided conductors (braiding attenuates/eliminates the effects of magnetic induction) allows to determine the following empirical equations for the example of steel and aluminium conductors with three layers of Aluminium (Zebra 428-A1 / S1A-57/7):

$$I_{DC} = I_{AC} \times \sqrt{1.0123 + 2.36 \times 10^{-5} \times I_{AC}} \quad (6)$$

This relation accounts for all the contributions described above for the Joule heating effect while for steel core conductors the current heating calculation is based on the equation relating the alternating and continuous input power for the same average conductor temperature [1]:

$$I_{AC}^2 R_{AC} = I_{DC}^2 R_{DC} \quad (7)$$

That after some manipulation leads to:

$$k_j = \frac{R_{AC}}{R_{DC}} = 1.0123 + 2.36 \times 10^{-5} \times I_{AC} \quad (8)$$

And thus:

$$P_j = (1.0123 + 2.36 \times 10^{-5} \times I_{AC}) I_{AC}^2 R_{DC} [1 + \alpha(\bar{T} - 20)] \quad (9)$$

The value k_j from equation (8) **Error! Reference source not found.** corresponds to a general formulation of the coefficient and if the effects of the alternate current are eliminated the value of $k_j = 1.0123$ then represent the skin effect of equation (5).

2.1.3 Solar heating

The solar thermal gain, P_S , depends on the conductor diameter (and for small conductor lengths, of its slope relative to the horizontal plane), the solar absorptivity of the conductor surface, α_S , the intensity of direct solar radiation on a surface normal to the solar rays, I_D , and the diffuse radiation intensity in the horizontal plane, I_d , the solar height h_S , the angle of incidence of the solar rays relative to the axis of the conductor, η , and the albedo of the surrounding the conductor surface [11], [17].

However, the present work uses, according to [16], an equation for the solar thermal gain, P_S , the heating due to the solar effect given by:

$$P_S = \alpha_S \times S \times D \quad (10)$$

where:

α_S – Solar absorptivity of the conductor surface;

S – global solar radiation intensity (W/m²);

D – outer diameter of the conductor (m).

The solar absorptivity of the conductor surface has values between 0.23 and 0.95, and for most applications, 0.5 is the norm for new cables [13], after one or two years of high voltage operation 0.8 should be used [1]. The latter is the value used in the present work

2.1.4 Corona heating

The American Standards Association defines the crown effect as a light electric discharge due to air ionization present in the vicinity of an electric conductor around which there is a voltage gradient that exceeds a certain critical value [17]. This discharge is observed on the surface of the conductor by the formation of an avalanche of electrons when the electric field strength at the conductor surface exceeds a given critical value [18], [19].

The crown heating of the conductor is only significant in the presence of high electric voltage gradients occurring during periods of precipitation and high wind speeds, *i.e.* when the convective and evaporative cooling is high. Due to this fact and since it is considered necessary to evaluate the limit of maximum transport capacity of the power lines based on unfavourable meteorological conditions (*i.e.*, favouring the heating of the electric conductors), the inclusion of the crown heating calculation is considered unnecessary and therefore does not contain a formulation for its computation [1]. According to CIGRÉ, the heating produced by the corona effect is considered cancelled by the evaporative effect and made irrelevant by convective high values, which are characteristic of the weather conditions that trigger the occurrence of the corona effect [20].

2.2 Cooling Effects

2.2.1 Convective cooling

The conductor's (hot) surface heats the air adjacent to it. This layer of heated air is separated from the conductor by convection through two different mechanisms. One is due to the decreased density value of the heated air which causes an upward movement designated as natural convection, $v = 0$, the other when the air is moved away from the surface of the conductor by the action of the wind designated by forced convection, usually for wind velocities above 0.5m/s. The adjacent hot air is, by the described phenomena, replaced by air at a lower temperature which cools the conductor [1], [15].

To evaluate the heat transfer by convective phenomena, it requires defining a set of non-dimensional parameters, the Nusselt number [15], Nu , Reynolds number, Re , Grashof number [1], Gr , and Prandtl number [15], Pr , respectively given by:

$$Nu = h_c \times D / \lambda_f \quad (11)$$

Where h_c is the heat transfer coefficient by convective effect (W/m), and λ_f is the thermal conductivity of the air (W/mK);

$$Re = \rho_r \times v \times D / \nu_f \quad (12)$$

where v is the wind speed (m/s), ν_f is the kinematic viscosity of the air (m²/s) and ρ_r is the normalization factor of the air density ($\rho_r = \rho / \rho_0$, where ρ is the air density for the altitude of the cable² in question and ρ_0 is the density of air at sea level);

$$Gr = [D^3 \times (T_s - T_a) \times g] / [(T_f + 273,15) \times \nu_f^2] \quad (13)$$

where T_s is the conductor surface temperature and T_a is the ambient temperature; and

$$Pr = c_{p_{ar}} \times \mu / \lambda_f \quad (14)$$

where $c_{p_{ar}}$ is the specific thermal capacity of air at constant pressure (J/kgK) and μ is the dynamic viscosity of air (kg/ms).

The variables mentioned above are, according to [1], given by the following empirical equations:

$$\nu_f = \mu / y \quad (15)$$

$$\mu = 0.17 \cdot 10^{-6} + 4.635 \cdot 10^{-8} \cdot T_f - 2.03 \cdot 10^{-11} \cdot T_f^2 \quad (16)$$

$$\lambda_f = (2,42 \times 10^{-2}) + (7,2 \times 10^{-5}) \times T_f \quad (17)$$

$$y = \frac{1.293 - 1.525 \cdot 10^{-4} \text{ altitude} + 6.379 \cdot 10^{-9} \text{ altitude}^2}{1 + 0.00367 \cdot T_f} \quad (18)$$

$$Pr = 0,715 - (2,5 \times 10^{-4}) \times T_f \quad (19)$$

² Soil altitude plus cable height.

$$g = 9,807 \text{ m/s}^2 \quad (20)$$

$$T_f = \frac{1}{2} \times (T_s + T_a) \quad (21)$$

$$\rho_r = e^{-1,16 \times 10^{-4} \times \text{altitude}} \quad (22)$$

ρ_r is the air density at a given altitude, considering the air density at sea level.

Convective cooling is computed by [21]:

$$P_c = \pi \times \lambda_f \times (T_s - T_a) \times Nu \quad (23)$$

The determination of the Nusselt number will depend on the type of convection (natural or forced), as will be presented below.

2.2.2 Forced convective cooling

For the normal temperature range of the air film adjacent to the conductor, $T_f = 0,5 \times (T_s + T_a)$, the Nusselt number can be determined by [1]:

$$Nu = B_1 \times (Re)^n \quad (24)$$

Where B_1 and n are constants dependent on the Reynolds number and the roughness of the conductor, R_f , given by

$$R_f = \frac{d}{2 \times (D - d)} \quad (25)$$

Table 1: Constants for calculation of forced convection on braided conductors cooled by constant airflow [1].

	Re	B_1	n
All surfaces	10^2 to 2.65×10^3	0.641	0.471
$R_f \leq 0,05$	$> 2.65 \times 10^3$ to 5×10^4	0.178	0.633
$R_f > 0,05$	$> 2.65 \times 10^3$ to 5×10^4	0.048	0.800

The non-ferromagnetic conductor cable is assumed to have an outside diameter d for each wire while the diameter D represents the overall diameter of the conductor.

The direction of the wind, *i.e.* the angle of incidence of the wind on the conductor's axis (angle of incidence), is of the utmost importance in the effectiveness of the forced convective cooling process since the Nusselt number varies with the sine of the angle of attack δ [1].

$$Nu_{\delta} = Nu_{90} \times [A_1 + B_2 \times (\sin \delta)^{m_1}] \quad (26)$$

Table 2: Constants for the calculation of the Nusselt number as a function of the angle of incidence of the wind [1].

	A_1	B_2	m_1
$0^{\circ} < \delta < 24^{\circ}$	0.42	0.68	1.08
$24^{\circ} \leq \delta \leq 90^{\circ}$	0.42	0.58	0.90

It should be noted that when the wind has a direction parallel to the conductor axis, *i.e.*, $\delta = 0^{\circ}$, the Nusselt number has a value of $0,42Nu_{90}$, 42% of the value it would present for an incidence angle of $\delta = 90^{\circ}$. This contribution is due to the turbulence of the airflow caused by the roughness of the conductor braid.

According to the CIGRE report [1], for wind speeds below 0,5 m/s, it is possible to demonstrate that there is no preferred wind direction, so the incident angle of the forced convections is fixed to 45° . Thus, the corrected Nusselt number, Nu_{cor} , is given by:

$$Nu_{cor} = Nu_{45} \quad (27)$$

2.2.3 Natural convective cooling

The Nusselt number for the natural convection cooling depends on the Rayleigh number (product of the numbers of Prandtl and Grashof) [1];

$$Nu = A_2 \times (Gr \times Pr)^{m_2} \quad (28)$$

Table 3: Constants for computing natural convection in air conductors [1].

$Gr \times Pr$	A_2	m_2
10^{-1} to 10^2	1.020	0.148
10^2 to 10^4	0.850	0.188
10^4 to 10^7	0.480	0.250
10^7 to 10^{12}	0.125	0.333

2.2.4 Convective cooling at reduced wind speeds

For reduced wind speeds ($v < 0,5 \text{ m/s}$) the cooling calculation may take into account a simultaneous presence of forced and natural convection. However, the literature suggests a methodology in which two cooling values are determined, to allow choosing the largest one of these [1].

$$Nu = \max(Nu_{NC}, Nu_{45}) \quad (29)$$

2.2.5 Radiative cooling

The thermal losses due to the radiative effect usually represent a reduced fraction of the total thermal losses contributing to conductor cooling, so it generally suffices to determine them by. [1],[15],[22]

$$Pr = \pi \times D \times \varepsilon \times \sigma_B \times [(T_s + 273,15)^4 - (T_a + 273,15)^4] \quad (30)$$

where ε , the emissivity of the conductor, varies between 0.23 for new conductors and 0.95 for industrial conductors with atmospheric exposure (the current literature recommends the use of 0.8), σ_B is the Stefan-Boltzmann constant ($5.67 \times 10^{-8} \text{ W/m}^2\text{K}^4$), T_s and T_a are the conductor surface temperatures and ambient in °C, respectively [1].

2.2.6 Evaporative cooling

The evaporative effect, since the conductor is in the presence of water vapour in the air, or of water drops around him, does not significantly alter the value of the cooling. This type of thermal loss can, however, represent a significant change in conductor cooling in situations of high precipitation (conductor completely encased in water), although in these situations this effect is compensated by an increase in the corona effect. For the reasons

given, and as suggested by the CIGRÉ report, the evaporative effect is usually ignored and will therefore not be taken into account [1], [2], [20].

2.3 Wind incident angle on overhead lines

Since some power lines have significant extensions (sometimes of hundreds of kilometres), the ambient meteorological conditions of the electric line may present significant variation along their route, so it is important to determine the set of meteorological variables values along that line that are most limiting for the lines' thermal balance. The method used to implement it uses the information from the vertices towers to split the network lines into n segments which in turn defines the spatial resolution for the meteorological data used. Each line segment is then assumed to experience the hourly meteorological conditions extracted from the NWP model for its central (mid-distance) point, over an entire year.

The angle of incidence of the wind on the conductor is determined by the difference between the direction of the wind and the direction of the conductor. The wind direction provided from the meteorological data is referenced to the geographic East, *i.e.*, in the meteorological data, the 0° corresponds to the Westerly flow. The direction of the conductor is computed from the vertex towers' coordinates. The CIGRÉ formulation was designed for angles up to 90° , because of the experimental trials that lead to the constants defined in Table 2. However, it is possible to use the model up to 180° because of the presence of the trigonometric function \sin in equation (26). Given that both the wind direction and the conductor orientation are converted to values between 0° and 180° , for each segment, then assuming that the conductor orientation (ξ) is represented by a straight line it is possible to compute the angle of incidence of the wind (δ) in the conductor, based on the wind direction (θ) by using (31).

$$\delta = \theta - \xi \quad (31)$$

The assumption that the sectors are defined by the vertice towers with general cartesian coordinates (x_1, y_1) and (x_2, y_2) allow the conductor's orientation to be assessed by:

$$\xi = \arctan\left(\frac{y_2 - y_1}{x_2 - x_1}\right) \quad (32)$$

3. Optimal power flow

A mathematical model to optimize the power flows on the overhead electric lines of a power grid of a general power system was developed at LNEG outside the scope of this project [11]. The optimized power flow model (OPF) was further developed and embedded with the DLR methodology developed within this project. The presentation of the OPF model programmed in GAMS® (General Algebraic Modelling System) can be found in [23]. The OPF mathematical model uses the traditional power flow formulation for active and reactive power flow per line and transformer.

From $i \rightarrow j$:

$$P_{ij} = \left[\frac{V_i^2}{m_{ij}^2} G_{ij} - \frac{V_i V_j}{m_{ij}} (G_{ij} \cos(\theta_i - \theta_j) + B_{ij} \sin(\theta_i - \theta_j)) \right] \forall_{ij} | line_{ij} = 1 \quad (33)$$

$$Q_{ij} = \left[\frac{V_i^2}{m_{ij}^2} (B_{ij} + Btr_{ij}) - \frac{V_i V_j}{m_{ij}} (B_{ij} \cos(\theta_i - \theta_j) - G_{ij} \sin(\theta_i - \theta_j)) \right] \forall_{ij} | line_{ij} = 1 \quad (34)$$

From $j \rightarrow i$:

$$P_{ji} = \left[V_j^2 G_{ij} - \frac{V_i V_j}{m_{ij}} (G_{ij} \cos(\theta_j - \theta_i) + B_{ij} \sin(\theta_j - \theta_i)) \right] \forall_{ij} | line_{ij} = 1 \quad (35)$$

$$Q_{ji} = \left[V_j^2 (B_{ij} + Btr_{ij}) - \frac{V_i V_j}{m_{ij}} (B_{ij} \cos(\theta_j - \theta_i) - G_{ij} \sin(\theta_j - \theta_i)) \right] \forall_{ij} | line_{ij} = 1 \quad (36)$$

where P_{ij} and P_{ji} are the active power flow of line, whenever declared existing ($line_{ij} = 1$), from node i to j and node j to i , respectively. Q_{ij} and Q_{ji} are the reactive power flows from node i to j and node j to i , respectively, V_i and V_j are the effective voltages at node i and j , respectively. θ_i and θ_j are the voltage phases at node i and j , respectively. m_{ij} is the tap transformer primary turns ratio, in the case of a line or a nominal

transformer $m_{ij} = 1$, G_{ij} and B_{ij} are the longitudinal conductance and susceptance between nodes i and j . Btr_{ij} is half of the transversal susceptance of the line between nodes i and j , so it is 0 in the case of a transformer.

The apparent power flows between nodes, S_{ij} and S_{ji} , are computed as follows.

From $i \rightarrow j$:

$$S_{ij} = \sqrt{P_{ij}^2 + Q_{ij}^2}, \quad \forall_{ij} |line_{ij} = 1 \quad (37)$$

From $j \rightarrow i$:

$$S_{ji} = \sqrt{P_{ji}^2 + Q_{ji}^2}, \quad \forall_{ij} |line_{ij} = 1 \quad (38)$$

Furthermore, considering the active and reactive generation, P_{Gi} , Q_{Gi} , and load, P_{Li} , Q_{Li} , and the (technical) activation of shunt capacitor banks, Q_{Ci} , the OPF model is based on a pair of power balances per each node i , one for the active power and another for the reactive power balance, considering the following formulation:

$$\sum_g^{G_i} P_{Gg} - \sum_l^{L_i} P_{Ll} - \sum_j^{J_i} P_{ij} = 0 \quad (39)$$

$$\sum_g^{G_i} Q_{Gg} - \sum_l^{L_i} Q_{Ll} + \sum_c^{C_i} Q_{Cc} - \sum_j^{J_i} Q_{ij} = 0 \quad (40)$$

G_i , L_i , C_i and J_i are, respectively, the number of generators, g , loads, l , capacitor banks or shunts, c , and lines j , connected to node i , respectively. These equations are complemented by a set of constraint equations to impose the technical conditions and operational limits. Generators have their own active and reactive power minimum, P_{Gg}^{min}

and $Q_{G_g}^{min}$, and maximum, $P_{G_g}^{max}$ and $Q_{G_g}^{max}$, limits, such as the reactive power limits of the capacitor banks, $Q_{C_c}^{min}$ and $Q_{C_c}^{max}$:

$$P_{G_g}^{min} \leq P_{G_g} \leq P_{G_g}^{max} \quad (41)$$

$$Q_{G_g}^{min} \leq Q_{G_g} \leq Q_{G_g}^{max} \quad (42)$$

$$Q_{C_c}^{min} \leq Q_{C_c} \leq Q_{C_c}^{max} \quad (43)$$

Other constraints like minimum and maximum node tensions and transformer ratios of each transformer, $V^{min}, V^{max}, m_{ij}^{min}$ and m_{ij}^{max} , frequency and the phase difference between nodes limit, $Dphase$, are general, constant and defined by TSOs accordingly to security reasons, considering the following formulation:

$$V^{min} \leq V_i \leq V^{max} \quad (44)$$

$$m_{ij}^{min} \leq m_{ij} \leq m_{ij}^{max} \quad (45)$$

$$-Dphase \times \frac{\pi}{180} \leq \theta_i - \theta_j \leq Dphase \times \frac{\pi}{180} \quad (46)$$

$$-Dphase \times \frac{\pi}{180} \leq \theta_j - \theta_i \leq Dphase \times \frac{\pi}{180} \quad (47)$$

Traditionally, apparent power constraints are defined seasonally by the TSO using a SLR methodology where the (design) meteorological conditions are extreme and constant. Using a DLR methodology allows to dynamically change the (hourly or another time step) values of those constraints, feeding the OPF model with apparent power limits using forecasts or close to real-time meteorological data. Transformers apparent power constraints are defined accordingly to their static design ratings. Accordingly, the apparent power limits of lines and transformers, S_{ij}^{lim} are defined using the following formulation:

$$\begin{aligned} S_{ij} &\leq S_{ij}^{lim}, \\ S_{ji} &\leq S_{ji}^{lim}, \\ S_{ij}^{lim} &= S_{ji}^{lim} \end{aligned} \quad (48)$$

The main difference between the OPF and the traditional power flow methodologies lies in the use of objective functions, enabling TSOs to minimize active or reactive power losses, P_{loss} or Q_{loss} , respectively, presented as follows:

$$P_{loss} = \sum_{i,j} \left[\left(\frac{V_i^2}{m_{ij}^2} + V_j^2 \right) - 2 \frac{V_i V_j}{m_{ij}} \cos(\theta_j - \theta_i) \right] G_{ij}, \quad \forall_{ij} |line_{ij}| = 1 \quad (49)$$

$$Q_{loss} = \left| \sum_{i,j} - \left[\left(\frac{V_i^2}{m_{ij}^2} + V_j^2 \right) (B_{ij} + B_{tr_{ij}}) - 2B_{ij} \frac{V_i V_j}{m_{ij}} \cos(\theta_j - \theta_i) \right] \right|, \quad \forall_{ij} |line_{ij}| = 1 \quad (50)$$

Therefore, considering the objective function and all technical limits, using the OPF with an SLR methodology all variables are optimized according to the real-time consumption and generation of the power system while using the OPF with a DLR methodology will also take into consideration the real-time values of the weather-sensitive variables of each line, presented in Section 2. The model leads to a Non-Linear Problem (NLP) that is initialised by a Linear Problem from simplified models. The initial model is the direct current model, a linear model where all nodes' voltage is equal to 1 p.u., the phase differences between nodes is close to zero and does not consider power losses. The results from this model may serve as initiating input directly to the main program or, if further data refinement is needed, to the intermediary model³ that solves the active power balance by only considering that all nodes voltage equal to 1 p.u. The complete model is then initiated with the results of the initial/intermediary model. The mathematical model was implemented in GAMS® (General Algebraic Modelling System). In [11], [23], was tested with several examples by comparing its results with the ones given by a commercial platform, PSSE® and using the validation examples from IEE The results differences were lesser than 1% while imposing the same conditions defining the steady-state,

³ This intermediary step may be proven unnecessary for the great majority of the cases, and the complete model may then be initialised by the linear model values.

4. Assessment of dynamic electric line capacity using optimal power flow

In the scope of this deliverable, a model is being built to perform a Dynamic Line Rate analysis on the power lines of an electric power system integrating high levels of energy production from wind or other variable renewable resources. The inherent variability of those renewable sources may, given the proper conditions, congest the existing power lines. DLR analysis is one of the less expensive and practical ways of overcoming the problems arising from those potential congestions [3].

4.1 The Benefits of a coupled DLR and OPF model

The power system benefits from coupling DLR and OPF derive from a more efficient long-term (several years) internal grid expansion planning, such as long-term planning of the tie-lines capacity. It also benefits the system by considering a better long to middle term (from one year to a month) planning of the monthly capacities of the transmission lines, especially the tie-lines. A conservative forecast methodology to compute the meteorological data is needed to feed the DLR methodology and it is also important to compute the day-ahead and intraday lines and tie-lines capacity, avoiding market splitting and conservative management of local congestions. During close to real-time operation is possible to use a pre-solve methodology not only to identify the critical sector of each line, but also to detect if the foreseen capacity of each line is lower than expected, which is important as a risk mitigation measure to avoid the operation of the lines above their thermal limits, guaranteeing their security, and avoiding possible shortages, or extra costs with the congestion management.

Figure 1 resumes the temporal applications of the coupled DLR and OPF model.

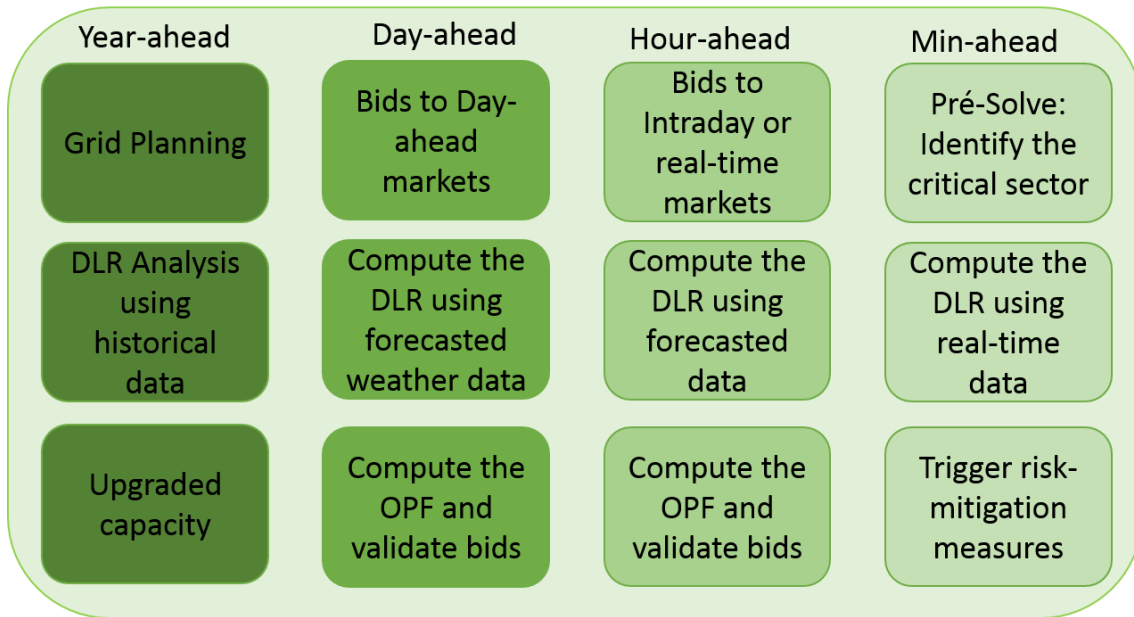


Figure 1: Temporal applications of the coupled DLR and OPF framework.

4.2 The coupled model framework

To facilitate the computations needed to obtain the data required by the DLR analysis it was decided to use georeferenced data of the power grid layout and the meteorological conditions. Given the expertise of some of the project team members, Matlab software was chosen to test the model. Taking into consideration future uses, this model has been developed to obtain solutions for long-term planning purposes, from years in case of grid expansion plans to the definition of the day-ahead line's capacity to the short-run close to the real-time operation of the lines. A schematic representation of the model and the information flow foreseen in this project is presented in Figure 2.

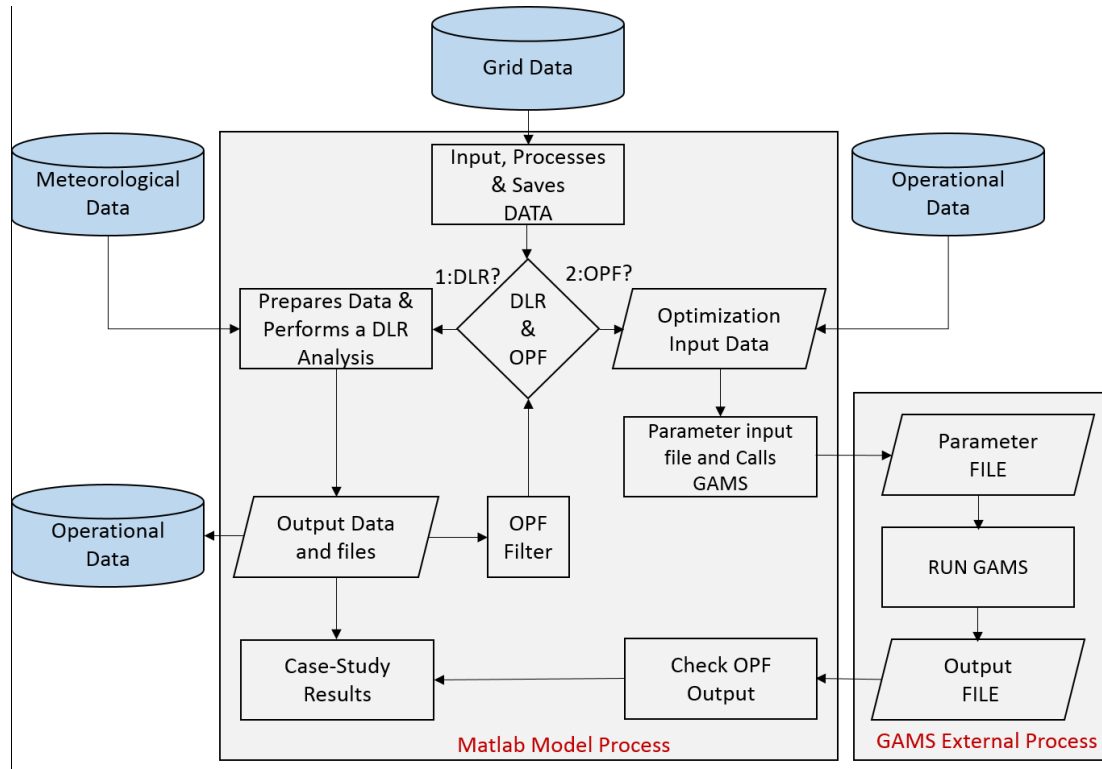


Figure 2: A schematic representation of the coupled model.

This model receives all input data and performs all the computations needed. It allows to:

1. Manage all required data:
 - a. Input the georeferenced data for the power grid under study;
 - b. Input all required parameters needed for both methodologies;
 - c. Input all saved results from previous DLR and OPF Analysis;
 - d. Graphically present the power grid under analysis;
2. Let the user define if wants to perform a DLR, an OPF Analysis, or both:
 - a. Select the required simulation, the region under study and the time horizon;
 - b. The model starts to identify the user selection by first verifying if a DLR Analysis is required and in case of yes, goes to step 3. Otherwise, it goes to step 4.
3. Perform a DLR Analysis:
 - a. Input the georeferenced data for the meteorological conditions;
 - b. Prepare all the data needed to perform both an SLR or a DLR analysis;
 - c. Perform the DLR Analysis and save its output in the case-studies results file, updating the operational data;

- d. Prepare the results to use in future OPF simulations;
 - e. Present the case-studies results.
4. Perform an OPF Analysis:
- a. Input the case-study operational data;
 - b. Use internal data in case of a coupled simulation, receives SLR and DLR operational results in case of only an OPF simulation;
 - c. Prepare all the data needed to a general OPF mathematical model, mainly the GAMS parameter input file;
 - d. Optimize the power flow for the selected power grid, by background calling the GAMS;
 - e. Write the optimized values to a file.

The coupled framework can be adapted to the temporal applications of the model defined in the previous section, as illustrated in Figure 3.

A long-term optimization process using DLR and OPF can be used as a decision support measure to decide for a possible grid expansion, or transportation lines and tie-lines upgrades, considering historical weather data and technical constraints to compute the DLR, such as the OPF to check for possible local congestions. Currently, some TSOs use seasonal or monthly reference weather data to compute the tie-lines capacity of their lines. DLR can be used to better compute these capacities instead of using static references.

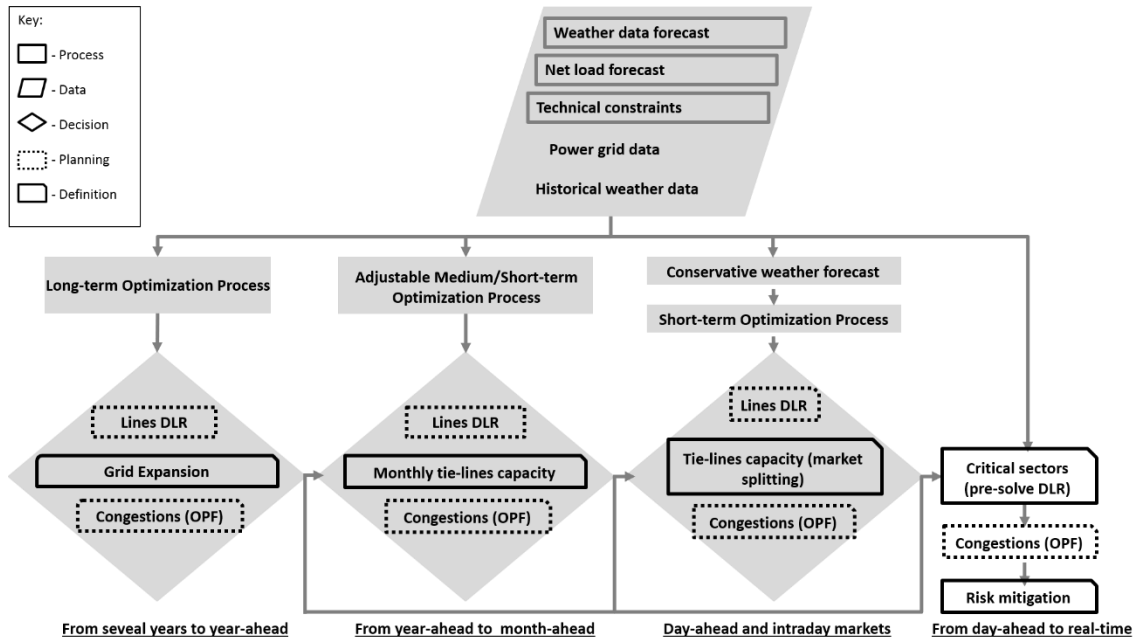


Figure 3: Temporal application of the coupled DLR and OPF framework.

Some power systems increase their costs because of market splitting and re-dispatching issues. Before day-ahead and intraday markets reliable conservative weather forecast methodologies can be used to feed the DLR model, computing the DLR of each line, that is used to feed the OPF model. The OPF model then checks the feasibility of the day-ahead and intraday deals, avoiding market splitting. A close to real-time analysis is very important to evaluate if the pre-computed capacities of the lines are overvalued, which put the security of the lines at risk. Using a pre-solve methodology it is possible to compute the critical sector of the line and verify if it is overvalued. Considering this case and the case when is needed to verify if exists some extra short-run capacity in specific lines, is possible to compute the DLR capacity of the lines' critical sectors, using this value to feed the OPF model, if needed.

To test the single and coupled models, the case studies used the data presented in deliverables from Task 2.

5. Final remarks

This deliverable presents the DLR methodology adopted that along with the upgraded OPF model (adapted for this project) may alleviate congestions in future power systems with high penetrations of renewable energy.

Based on the models previously developed by LNEG, some improvements were incorporated to include relevant key features enabling the use of DLR in real-time operation. These features include *i)* an iterative process with a 1h time step over the 24h time horizon fed by a day-ahead meteorological forecast data; and *ii)* the development of each model (DLR and OPF) in a way that allows their integration into a single coupled model, allowing to test the models and to perform the simulations. These improvements were tested using part of the data obtained from Task 2, to assess the ampacity for the case studies lines that, according to prior network optimization analysis, were identified as the ones approaching their stipulated ampacity limits. Nevertheless, a more complete analysis of the benefit of the models under development will only be performed in Task 5.

6. References

- [1] J. Iglesias *et al.*, ‘Guide for thermal rating calculations of overhead lines’, *CIGRÉ WG B2.43*, p. 93, 2014.
- [2] IEEE Power Engineering Transmission and Distribution, ‘IEEE Standard for Calculating the Current-Temperature of Bare Overhead Conductors’, *IEEE Std 738-2006 (Revision of IEEE Std 738-1993)*, pp. 1-59, 1 2007.
- [3] C. J. Wallnerstrom, Y. Huang and L. Soder, ‘Impact from Dynamic Line Rating on Wind Power Integration,’ *IEEE Transactions on Smart Grid*, Bd. 6, pp. 343-350, 2015.
- [4] S. Talpur, C. J. Wallnerstrom, P. Hilber und C. Flood, ‘Implementation of Dynamic Line Rating in a Sub-Transmission System for Wind Power Integration’, *Smart Grid and Renewable Energy*, pp. 233-249, 2015.
- [5] E. Fernandez, I. Albizu, M. T. Bedialauneta, A. J. Mazon und P. T. Leite, ‘Review of dynamic line rating systems for wind power integration’, *Renewable and Sustainable Energy Reviews*, Bd. 53, pp. 80-92, 2016.

- [6] Â. Casaleiro, ‘Modelação de Redes Elétricas Congestionadas’, *Master thesis at Faculdade de Ciências – Mestrado Integrado em Engenharia da Energia e do Ambiente (in portuguese)*, p. 101, 2015.
- [7] A. Medeiros, ‘Modelação dos parâmetros ambientais para a optimização da gestão de congestionamentos na transmissão de potência eólica’, *Master thesis at Faculdade de Ciências – Mestrado Integrado em Engenharia da Energia e do Ambiente (in portuguese)*, p. 94, 2016.
- [8] S. Raimundo, ‘Gestão Otimizada de uma Rede Eléctrica com Elevada Penetração Renovável e Análise Dinâmica da Capacidade das Linhas’, *Master thesis at Faculdade de Ciências – Mestrado Integrado em Engenharia da Energia e do Ambiente (in portuguese)*, p. 77, 2017.
- [9] CIGRE, ‘Compliance Guide of CIGRE report – Revised 2014/07/25’, p. 4, 2014.
- [10] A. Couto *et al.*, ‘Impact of the dynamic line rating analysis in regions with high levels of wind and solar PV generation’, in *2020 IEEE PES Innovative Smart Grid Technologies Europe (ISGT-Europe)*, pp. 1206-1210. IEEE, 2020.
- [11] A. Castanho, ‘Análise de Sensibilidade da Capacidade de Transporte da Rede Elétrica ao Aumento da Produção Renovável Distribuída: Desenvolvimento de Modelos de Otimização’, *Master thesis at Faculdade de Ciências – Mestrado Integrado em Engenharia da Energia e do Ambiente (in portuguese)*, p. 127, 2017.
- [12] CIGRÉ Working Group, ‘Thermal Behaviour Of Overhead Conductors’, Cigré, 2002, p. 45.
- [13] J. Fu, S. Abbott, B. Fox, D. J. Morrow and S. Abdelkader, ‘Wind cooling effect on dynamic overhead line ratings’, pp. 1-6, 2010.
- [14] C. F. Price and R. R. Gibbon, ‘Statistical approach to thermal rating of overhead lines for power transmission and distribution’, *Bd. 130*, pp. 245-256, 1983.
- [15] T. L. Bergman and F. P. Incropera, ‘Fundamentals of heat and mass transfer’, *7th Edition, 7th Hrsg.*, John Wiley & Sons, p. 1072, 2011.

-
- [16] P. A. Lynn, ‘Electricity from Sunlight: An Introduction to Photovoltaics’, *Chichester, : John Wiley & Sons, Ltd*, p. 221, 2010.
- [17] A. K. Deb, ‘Powerline ampacity system: theory, modeling and applications’, *1 Ed. Hrsg., CRC Press*, p. 264, 2000.
- [18] W. C. Lin and W. D. Caldwell, ‘Apparatus for preventing coronal discharge - US6455782 B1’, *Google Patents*, p. 8, 2002.
- [19] Hubbell Power Systems Inc., ‘What is corona? A clearly explained and illustrated story about three types of corona discharge and their relationship to radio interference’, *in Hubbell Power Systems Inc., Bulletin EU 1234-H*, p. 8, 2004.
- [20] N. P. Schimidt, ‘Comparison between I.E.E.E. and C.I.G.R.É. ampacity standards’, *IEEE Transactions on Power Delivery*, Bd. 14, pp. 1555-1559, 1999.
- [21] R. Stephen, D. Douglass and M. Gaudry, ‘Thermal behavior of overhead conductors’, 2002.
- [22] R. Petela, ‘Engineering Thermodynamics of Thermal Radiation: for Solar Power Utilization’, *McGraw-Hill Education*, p. 416, 2010.
- [23] J. Duque, A. Castanho and A. Estanqueiro, ‘Development of an Optimal Power Flow Model for maximum Variable Renewable Energy (VRE) Integration’, *in LNEG Tech. Report*, p. 40, 2016.